DENTAL MATERIALS 35 (2019) e163–e174

Available online at www.sciencedirect.com

ScienceDirect

journal homepage: www.intl.elsevierhealth.com/journals/dema

Electrochemical characterization of novel Ag-based brazing alloys for dental applications

Argiro Ntasi[a], *Youssef S. Al Jabbari*[b,c], *Wolf Dieter Mueller*[d], *Theodore Eliades*[e], *Spiros Zinelis*[a,b,*]

[a] *Department of Biomaterials, School of Dentistry, National and Kapodistrian University of Athens, Athens, Greece*
[b] *Dental Biomaterials Research and Development Chair, College of Dentistry, King Saud University, Riyadh, Saudi Arabia*
[c] *Prosthetic Dental Sciences Department, College of Dentistry, King Saud University, Riyadh, Saudi Arabia*
[d] *Dental and Biomaterials Research Group Dental School, "Charite" Medical University of Berlin, Germany*
[e] *Clinic of Orthodontics and Paediatric Dentistry, Center of Dental Medicine, University of Zurich, Zurich, Switzerland*

ARTICLE INFO

Article history:
Received 13 January 2019
Received in revised form
15 February 2019
Accepted 6 May 2019

Keywords:
Brazing
Electrochemical testing
Silver alloys
Corrosion

ABSTRACT

Objective. Taking into account that clinical data have proven the decomposition of Ag brazing alloys used in the production of orthodontic appliances the aim of this study was to develop new Ag based soldering alloys free of Cu and Zn.

Methods. Four commercially available Ag brazing alloys were selected and their electrochemical properties were compared to the following experimental alloys: Ag12Ga, Ag10Ga5Sn, Ag20In and Ag7Sn. 112 disk shape specimens were prepared for each alloy and their electrochemical properties were evaluated by Open Circuit Potential (OCP), linear sweep voltametry (LSV), cyclic polarization (CP) and electrochemical impedance spectroscopy (EIS) in a NaCl 0.9% and a Ringer's electrolyte solution.

Results. The experimental alloys combined higher OCP and E_{corr} with lower I_{corr} values. The impedance values of the commercial alloys were lower showing that any surface layers formed are not protective and steady compared to those of the novel ones. In conclusion experimental alloys demonstrated enhanced electrochemical properties.

Significance. In and Sn showed a more beneficial effect on electrochemical properties compared to Ga and thus can be considered as a promising option for the development of a new family of Ag brazing alloys with increased biocompatibility.

1. Introduction

Many orthodontic appliances are manufactured by joining dissimilar metallic parts and Ag brazing alloys are extensively used in the production of brackets, hyrax appliances, headgears, space maintainers and others [1–3]. The placement of a metallic material in the aggressive environment of the human mouth always raises concerns for the potential adverse biological consequences due to release of heavy metal ions through corrosion and/or wear mechanisms [4]. The fact that all commercially available Ag brazing alloys are based on the Ag–Zn–Cu ternary systems [5,6] reinforces the above mentioned concerns, as experimental studies on orthodontic

* *Corresponding author at*: Department of Biomaterials, School of Dentistry, National and Kapodistrian University of Athens, Thivon 2, Goudi 11527, Athens, Greece.
E-mail address: szinelis@dent.uoa.gr (S. Zinelis).
https://doi.org/10.1016/j.dental.2019.05.005

devices demonstrated that they are prone to Cu and Zn release [7–11]. Furthermore, the presence of a joint between dissimilar alloys triggers galvanic corrosion phenomena [12]. Berge et.al [8] demonstrated that open cell potentials between Ag brazing alloy and stainless steel (SS) alloys differ by 360 mV (much more than the threshold for galvanic actions 200 mV) with the solder being the anode (and thus is corroded) when the assembly is placed in the oral cavity. Recently the aforementioned concerns were verified by clinical studies. Freitas et.al [1] revealed the release in saliva of Cu, Zn and Cd ions 10 min, 1, 7, 30 and 60 days after the placement of hyrax appliances in patients while Sotiriou et.al [3] demonstrated the decomposition of the Ag joint of space maintainers by measuring the concentrations of Cu and Zn of Ag brazing alloys before and after orthodontic treatment.

The biological consequences of Cu uptake are associated with gastrointestinal irritation, liver damage [13] and atherogenesis [14].Also due to its ability to form reactive oxygen species (ROS), Cu may cause oxidative damage and induce carcinogenesis and neurodegenerating processes [13,15–18]. Additionally Zn may cause functional impairment in immunological response and reduce HDL cholesterol [19]. It may simultaneously induces sensitivity in Cloudman melanoma cells in vitro [20] and is proven to be cytotoxic for fibroblasts [21]. The degradation of Ag brazing alloys under clinical conditions has been associated with the early failure and the replacements of orthodontic appliances [22–27] exposing the patients to a second dose of released elements.

In order to overcome the aforementioned concerns and increase the biocompatibility of Ag joints, new brazing alloys should be developed free of Cu and Zn. Therefore, the aim of this study is the comparative analysis of electrochemical properties of contemporary and experimental Ag brazing alloys. The null hypothesis was that both experimental and commercial alloys will share equal electrochemical characteristics.

2. Materials and methods

2.1. Alloy and specimen preparation

Four commercially available Ag based brazing alloys were included in this study (Table 1) along with four experimental alloys fabricated in an induction-melting machine (Ducatron S3, UGIN'Dentaire, Seyssins, France) using a silicate crucible (UGIN'Dentaire) appropriate for melting precious alloys. The materials, which were inductively melted, were Ag 99.99 wt% (AG006105/4, Goodfellow, Huntingdon, England), Ga 99.99 wt% (S97020, Johnson Matthey GmbH, Karlsruhe, Germany), Sn 99.995 wt% (SN006102/4, Goodfellow) and In 99.99 wt% (9300, Johnson Matthey GmbH). Table 1 shows the elemental composition of the alloys used in the study.

An adequate amount of each alloy was melted in a reducing flame and placed in a mould, so as to fabricate 14 disc shape specimens of each material (112 in total). For melting Leo and Ort the fluxes provided by the manufacturers were used (Leone fluoride flux paste (Leone S.p.a, Italy), and Ortho Technology TruFlow Orthodontic Flux (Ortho Technology) respectively), whereas for Nob and Den the flux was included in the structure of the brazing wire as a separate layer. Then the specimens were conventionally ground with silicon carbide paper up to 4000 grit and polished with a diamond suspension (DiaPro suspension solution, Struers Ballerup, Denmark). Finally they were put in an ultra sonic bath with ethanol for 3 min and then rinsed with water and dried.

2.2. Electrochemical methods

The electrochemical methods used were Open Circuit Potential (OCP), Linear Sweep Voltammetry (LSV), Cyclic Polarization (CP) and Electrochemical Impedance Spectroscopy (EIS). All methods were accomplished with the use of a Mini Cell System (MCS). A Saturated Calomel Electrode (SCE) was used as a reference electrode and a platinum wire was used as an auxiliary electrode. The sampling area of the testing electrode was 0.008 cm^2. The assembly was connected to a computer controlled potentiostat (Voltalab/Radiometer Analytical PGZ402, Villeurbanne, Cedex, France). The electrolyte solutions used were Ringer's solution (9 g NaCl, 0.24 g $CaCl_2 \cdot 6H_2O$, 0.43 g KCl, 0.2 g $NaHCO_3$ in 1000 ml distilled water) and NaCl 0.9% and all measurements were carried out in ambient temperature.

2.2.1. Open circuit potential

The OCP was recorded for 5 min employing a logging rate of 1 measurement per sec. The data were collected and analyzed by using the Voltalab software.

2.2.2. Linear sweep voltammetry

LSV was performed over a potential range of −1000 to +1250 mV with a scan rate of 10 mV/s. The data were collected and analyzed by using the Voltalab software. The exchange current density (I_{corr}) and the corrosion potential (E_{corr}) were estimated after Tafel modeling. In order to create a mean curve for each material, the experimental curves were treated using Origin software.

2.2.3. Cyclic polarization

CP was performed with the abovementioned conditions and each measurement contained five scan cycles. The data were collected and analyzed by using the Voltalab software. In order to create a mean curve for each material, the experimental curves were treated using Origin software.

After CP the elemental composition of all alloys tested were determined by Scanning Electron Microscopy and X-ray Energy Dispersive Spectroscopy (SEM/EDX) analysis. The samples were examined using a scanning electron microscope (SEM) (Quanta 200, FEI, Hillsboro, OR, USA) equipped with an energy-dispersive X-ray spectrometer (Sapphire CDU, EDAX Int, Mahwah, NJ, USA). EDX spectra were recorded under high vacuum chamber conditions (10^{-6} mbar), 30 keV accelerating voltage, 108 μA beam current and 640 × 640 μm collecting window.

2.2.4. Electrochemical impedance spectroscopy (EIS)

EIS was performed in a frequency range from 70 KHz to 10 mHz with 10 points per decade and 15 mV wave amplitude. All measurements were conducted at OCP and 100 μA current range. The absolute impedance and phase angle were measured at each frequency so as to produce Nyquist.

Table 1 – Brand name, composition and code of the commercially and experimental alloys tested.

Brand name (Manufacturer)	Elemental composition (wt.%)	Code
Dentaurum Universal silver solder (Dentaurum, Ispringen, Germany)	Ag:59, Cu:16, Zn:25	Den
Leone R0224-00 (Leone Florence. Italy)	Ag:55, Cu:21, Zn:22, Sn:2	Leo
Nobil Metal Solder LV15 (Nobil Metal, Villa Franca d'Asti, Italy)	Ag:59, Cu:16, Zn:25	Nob
Ortho Technology silver solder #2020 (Ortho Technology Inc. Tampa, FL)	Ag:1.5-55, Cu:19-95, Zn:2-44, Ni:0.1-24	Ort
AgGa	Ag:88, Ga:12	AgGa
AgGaSn	Ag:75, Ga:10, Sn:5	AgGaSn
AgIn	Ag:80, In:20	AgIn
AgSn	Ag:93, Sn:7	AgSn

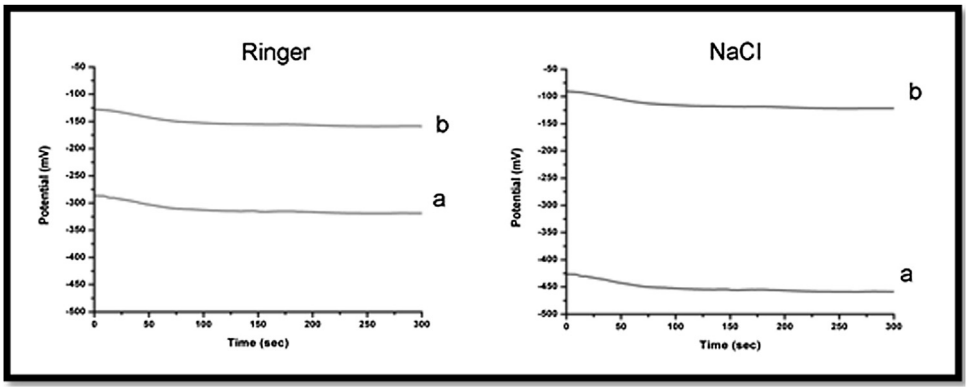

Fig. 1 – Representative OCP curves for commercial (a) (Leo in the diagram) and experimental (b) (AgGaSn in the diagram) alloys for both solutions tested.

2.3. *Statistical analysis*

The OCP, E_{corr} and I_{corr} values in each electrolyte were compared using One Way Analysis of Variance and pairwise multiple comparison (Holm–Sidak) at a = 0.05.

3. Results

3.1. *Open Circuit Potential (OCP)*

From Fig. 1, which shows the shapes of the OCP curves of the alloys tested shows that the potential begins from an initial value when t = 0 s and soon after decreases to a steady OCP voltage. In Fig. 2 the OCP values and their comparison in each solution are presented. The experimental alloys demonstrate significantly higher values than the commercially alloys. AgSn demonstrates the highest OCP value in Ringer's solution (Fig. 2a), whereas in NaCl, AgSn and AgGaSn display the highest ones (Fig. 2b).

3.2. *Linear sweep voltammetry*

Fig. 3 presents the LSV curves of the alloys tested in both solutions whereas in Table 2 the calculated I_{corr} and E_{corr} values are given. In both solutions experimental alloys statistically have significantly better E_{corr} and lower I_{corr} values than conventional ones. Among the experimental alloys, AgSn illustrated the higher E_{corr} and lower I_{corr} in both media (Table 2).

3.3. *Cyclic polarization*

The full first scanning cycle is presented in Figs. 4 and 5, for Ringer's and NaCl, respectively. Apart from Den and AgSn all the commerciall alloys tested demonstrate a continuous increase in current in forward scanning. Den demonstrates a tiny peak close to −100 mV (This is more visible in Figs. 6a and 7 a) and a broad peak at the range of 250 to 450 mV followed by a decrease in current at more anodic potentials. Among the experimental alloys, AgSn reaches a "plateau" at around 750 mV. The experimental alloys demonstrate a wider stability area in both solutions in the range of −750 to −50 mV, which is followed by an abrupt current increase. All alloys tested showed a negative hysteresis in reverse scanning, while the commercial alloys demonstrate a reduction peak at about −500 to −700 mV in Ringer's solution (Figs. 4a–d), which in the case of Den is wider and the current developed is remarkably higher (Figs. 4a and 5 a).

Irrespective of current magnitude alterations or peak shifting, the shape of the curves in the five successive cycles is the same and thus for simplicity only the forward scanning of the alloys tested in the respective solutions are shown in Figs. 6 and 7. In Den the current peaks shift in the anodic direction and increase consecutively from the first to the fifth cycle

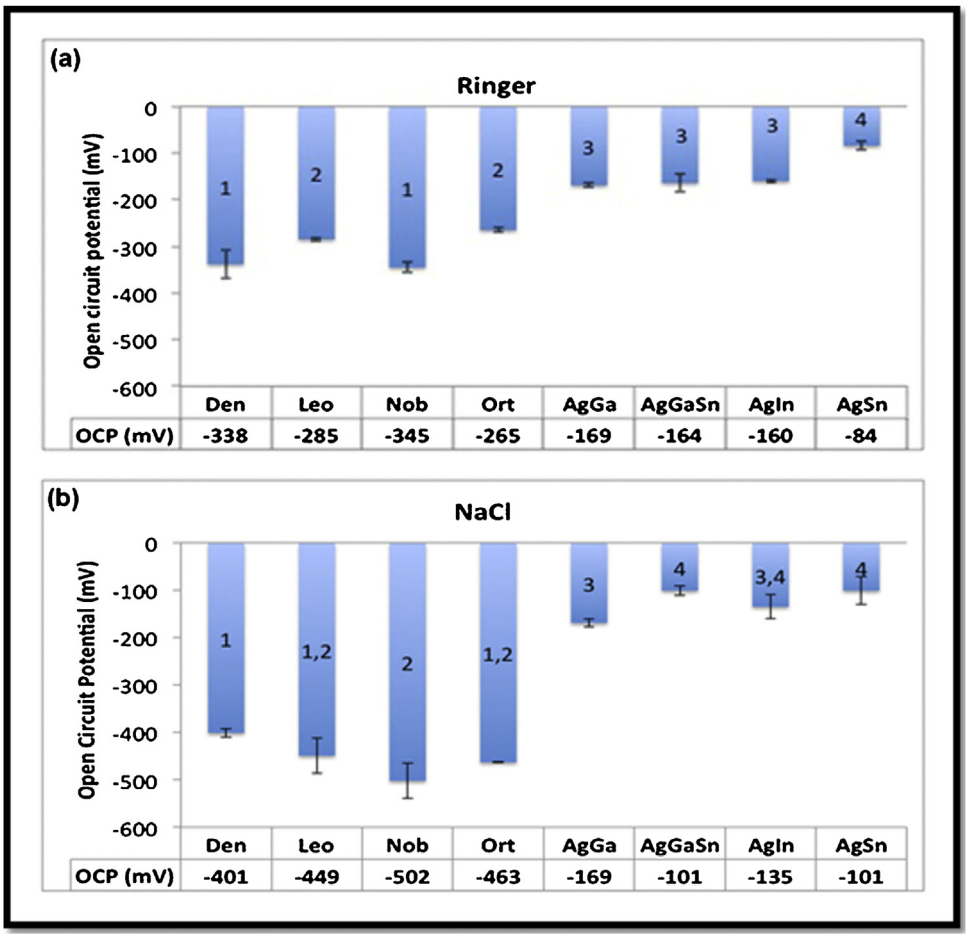

Fig. 2 – Comparison of the mean OCP values of all the alloys tested in Ringer's (a) and NaCl (b) solution. The mean value of OCP for each alloy is tabulated below each bar. The same number in the bars indicates mean values without statistical differences ($p > 0.05$).

(Figs. 6a and 7 a). Leo and Nob in Ringer's solution (Fig. 6b-c) show an increase of current density during the anodic part of forward scanning from the first to the fifth cycle. Apart from Den the behavior of the commercially alloys in NaCl is the same for the five scanning cycles (Figs. 6b–d). The experimental alloys demonstrate an anodic shift of the potential at which the passive region begins in successive cycles in both solutions, whereas the other curve characteristics of the anodic part remain the same (Figs. 6e–h and 7e–h).

The EDX results (Fig. 8) where Cl and O peaks were identified on all surfaces.

3.4. *Electrochemical impedance spectroscopy (EIS)*

The Nyquist plots for all alloys tested are shown in Fig. 9 for Ringer's (a) and NaCl (b). The shape of the curves is similar but the impedance values are impressively lower in the case of the commercially alloys.

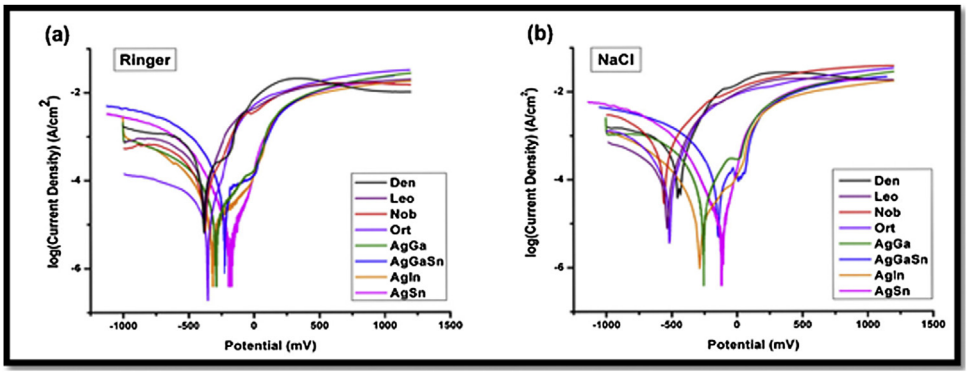

Fig. 3 – LSV curves of the alloys tested in Ringer's (a) and NaCl (b) media. The current density axis is in logarithmic scale.

Table 2 – Mean values of E_{corr} (mV) and I_{corr} (A/cm^2) with standard deviations in parentheses from all alloy tested in Ringer's and NaCl solutions.

	Ringer's		NaCl	
Alloy	E_{corr}	I_{corr}	E_{corr}	I_{corr}
Den	-401 ± 47^{a}	$2.6 \pm 1.8 \times 10^{-4\,a}$	-443 ± 19^{a}	$2.9 \pm 0.9 \times 10^{-4\,a}$
Leo	-352 ± 43^{a}	$3.7 \pm 2.7 \times 10^{-4\,a}$	-543 ± 9^{b}	$1.8 \pm 1.9 \times 10^{-4\,a}$
Nob	-385 ± 28^{a}	$1.2 \pm 0.4 \times 10^{-4\,a}$	-551 ± 13^{b}	$8.4 \pm 6.5 \times 10^{-4\,b}$
Ort	-363 ± 22^{a}	$7.3 \pm 0.5 \times 10^{-6\,b}$	-528 ± 28^{b}	$1.3 \pm 0.4 \times 10^{-4\,a,c}$
AgGa	-298 ± 24^{b}	$1.5 \pm 0.5 \times 10^{-5\,c}$	-255 ± 13^{c}	$2.9 \pm 1.6 \times 10^{-5\,d}$
AgGaSn	-203 ± 32^{c}	$2.7 \pm 1.8 \times 10^{-6\,d}$	-156 ± 19^{d}	$8.4 \pm 5.3 \times 10^{-5\,c}$
AgIn	-305 ± 18^{b}	$9.4 \pm 0.7 \times 10^{-6\,b,c}$	-271 ± 27^{c}	$8.9 \pm 0.5 \times 10^{-6\,e}$
AgSn	-194 ± 14^{c}	$4.9 \pm 3.6 \times 10^{-6\,d}$	-122 ± 21^{d}	$7.4 \pm 1.8 \times 10^{-6\,e}$

Different superscripts indicate statistical significant different values of E_{corr} or I_{corr} among materials tested.

4. Discussion

Based on the experimental results of this study the null hypothesis must be rejected as experimental alloys demonstrated enhanced electrochemical properties. In order to overcome the biological concerns of the silver brazing materials, experimental alloys were developed free of Cu and Zn. The alloying elements were selected based on the following criteria:

- Decrease of the melting point: The brazing alloy shall melt below the solidus temperature of stainless steel SS used in orthodontics to avoid melting of the joined parts.
- Microstructural constraint: To eliminate the selective leaching, the composition of the alloys selected should not exceed the maximum solubility in solid solution (as given by the binary phase diagrams) in order to provide a single phase material. The elimination of a second phase is the most promising way to increase the corrosion resistance of multiphase alloys.
- Cytotoxicity: The metal selected should not have been correlated with any adverse biological consequences.

Taking into account the above and the relevant phase diagrams, the experimental Ag brazing alloys (Table 1) were prepared employing only Ga, Sn and In in the selected formulations.

From the shape of the OCP curves of all alloys it seems that both experimental and commercial alloys quickly reach a constant value, implying the establishment of equilibrium between the developed surface oxide and solution. Furthermore the experimental alloys demonstrate higher OCP values, showing a more noble behaviour. In Ringer's solution the OCP values are higher for all alloys, as would be expected for a less aggressive solution.

For LSV and CP a sufficiently high scanning rate was selected in order facilitate the acquisition of an adequate number of spectra to get enough data for statistical comparisons. Since E_{corr} represents the potential at which current changes from cathodic to anodic direction, it is a thermodynamic characteristic of the redox reaction in the electrolyte solution and is independent of the specimens' kinetics. In the present study the commercially available alloys demonstrate statistically equal E_{corr} values in Ringer's solution and thus similar thermodynamic behavior, whereas in NaCl 0.9% the significantly higher E_{corr} for Den indicates that it is more difficult for this alloy to be oxidized. The values of E_{corr} and I_{corr} of commercial alloys are similar to previously reported values in same solutions [5]. Furthermore, the E_{corr} values of the experimental alloys are higher denoting lower corrosion vulnerability compared to the commercial ones. In Ringer's the E_{corr} values are shifted anodically resulting in higher corrosion immunity. Among the experimental alloys, AgSn exhibited the higher E_{corr} value, showing that a higher potential is needed for its oxidation. Since the experimental alloys demonstrate lower I_{corr} values the rate of the redox reaction is lower compared to that of the commercial ones.

According to Beverskogs' Pourbaix diagrams [28] for Cu at 25 °C and neutral pH, $CuCl_2^-$ ions are formed at −110 mV according to the two step anodic reaction [29–31]:

$$Cu + Cl^- \Leftrightarrow CuCl + e^- \quad \text{(R.1)}$$

$$CuCl + Cl^- \Leftrightarrow CuCl_2^- \quad \text{(R.2)}$$

while the formation of CuO in higher potentials (100 to 400 mV) results from according to the reaction [32]:

$$Cu^+ + H_2O \Leftrightarrow CuO + 2H^+ + e^- \quad \text{(R.3)}$$

Additionally, Ag is being oxidized to AgCl at around 250 mV (at the same potential that the second anodic peak of Cu is observed) forming a porous layer on the metal surface, according to the reaction [33]:

$$Ag + Cl^- \Leftrightarrow AgCl + e^- \quad \text{(R.4)}$$

From the above can be concluded that the small peak in the anodic branch of the voltammograms of the commercial alloys at −100 mV can be attributed to Cu oxidation [34,35], leading in the formation of a protective layer on the alloys' surface composed of Cu_2O, and/or $CuCl_2^-$. However the film is easily ruined as the current increases at higher potentials, especially for Leo Ort and Nob. The second wider peak that is observed in Den at 250–450 mV can be attributed to the contribution of CuO and AgCl formation ((R.3) and (R.4) respectively). However, from the anodic scans from the five cycles of the commercial alloys in Ringer's solution a second peak appears for Nob and Ort during the second scanning cycle and thus the corrosion

mechanism described for Den justifies the behavior of these alloys.

Since all commercially alloys demonstrate negative hysteresis during the CP measurements any pits created can repair themselves during reverse scanning. The peak at around −500 to −700 mV may be attributed to Cu reduction. The small shoulder that appears during reverse scanning for Den and Nob at 125 mV and 450 mV, respectively, in Ringer's solution suggests the initiation of a reactivation process, probably due to the absence of a compact continuous film on the alloy's surface [36]. The latter conclusion is reinforced by the SEM images were the depositions developed after potentiodynamic testing, probably hindering the formation of a uniform surface oxide film (Figs. 8 and 9). The formation of surface oxide and chloride films is reinforced by the presence of Cl and O concentration after the CP testing according to the results of EDX analysis (Figure 8).

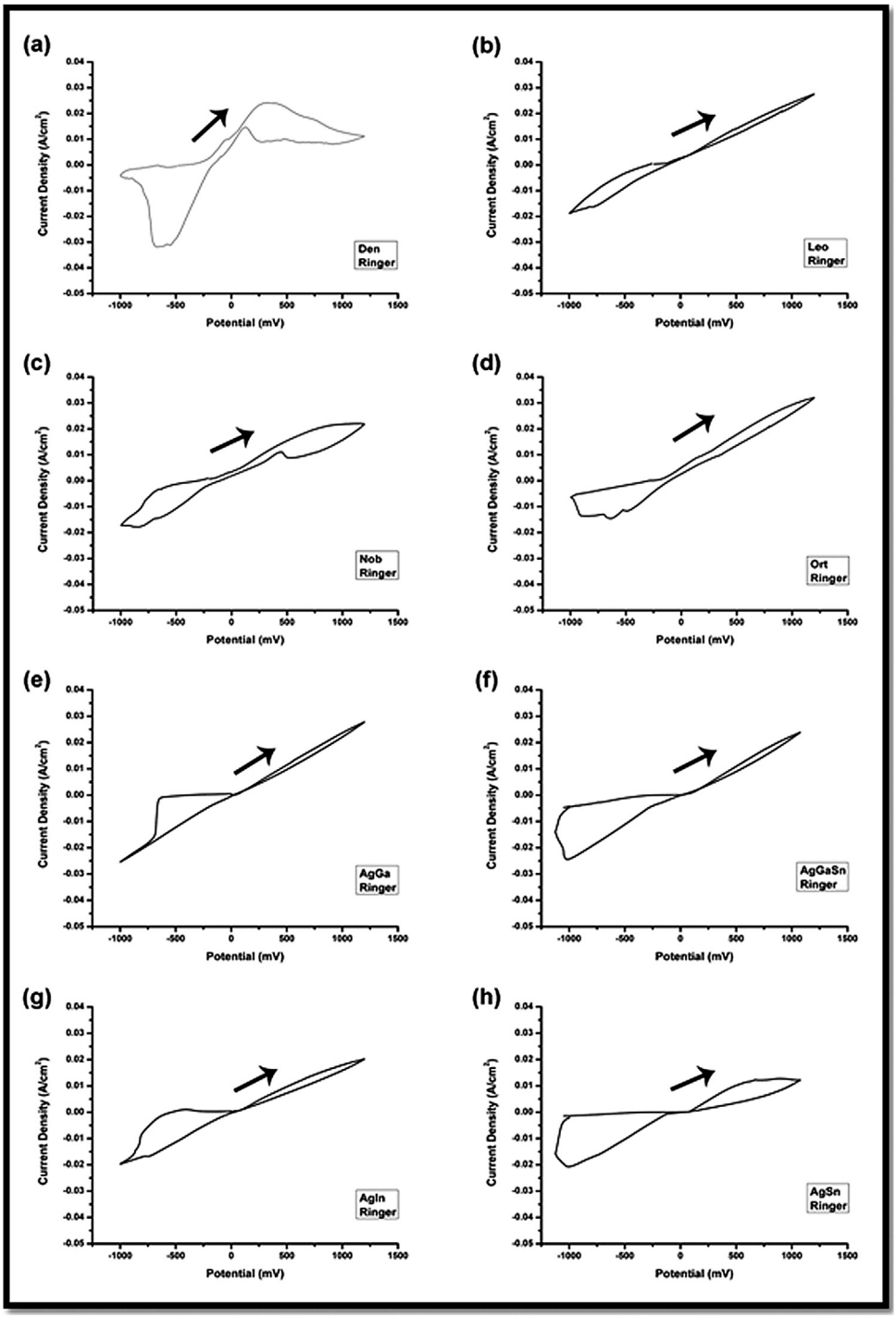

Fig. 4 – The first cycle for each alloy in Ringer's solution: Den (a), Leo (b), Nob (c), Ort (d), AgGa (e), AgGaSn (f), AgIn (g), AgSn (h).

The passive area AgGa alloy in both solutions can be attributed to the formation of a passive layer according to the reactions:

$$2Ga + 3H_2O \Leftrightarrow Ga_2O_3 + 6H^+ + 6e^- \quad (R.5)$$

$$Ga + xCl^- \Leftrightarrow GaCl_x + xe^- \quad (R.6)$$

Horasawa et al. [35] found that when Ga is immersed in a chloride solution (NaCl 1%) the main corrosion product is $GaCl_x$ instead of oxides and attributed this finding to the higher concentration of Cl^- compared to that of OH^- and to its tendency to form chlorides. The chloride film is soluble, and thus not steady. As such it can be easily destroyed at higher potentials as demonstrated by the CP curve (Fig. 7e).

For AgSn alloy at potentials around −600 to −400 mV the formation of a protective layer takes place according to the reactions R.7–R.12:

$$Sn \Leftrightarrow Sn^{2+} + 2e^- \quad (R.7)$$

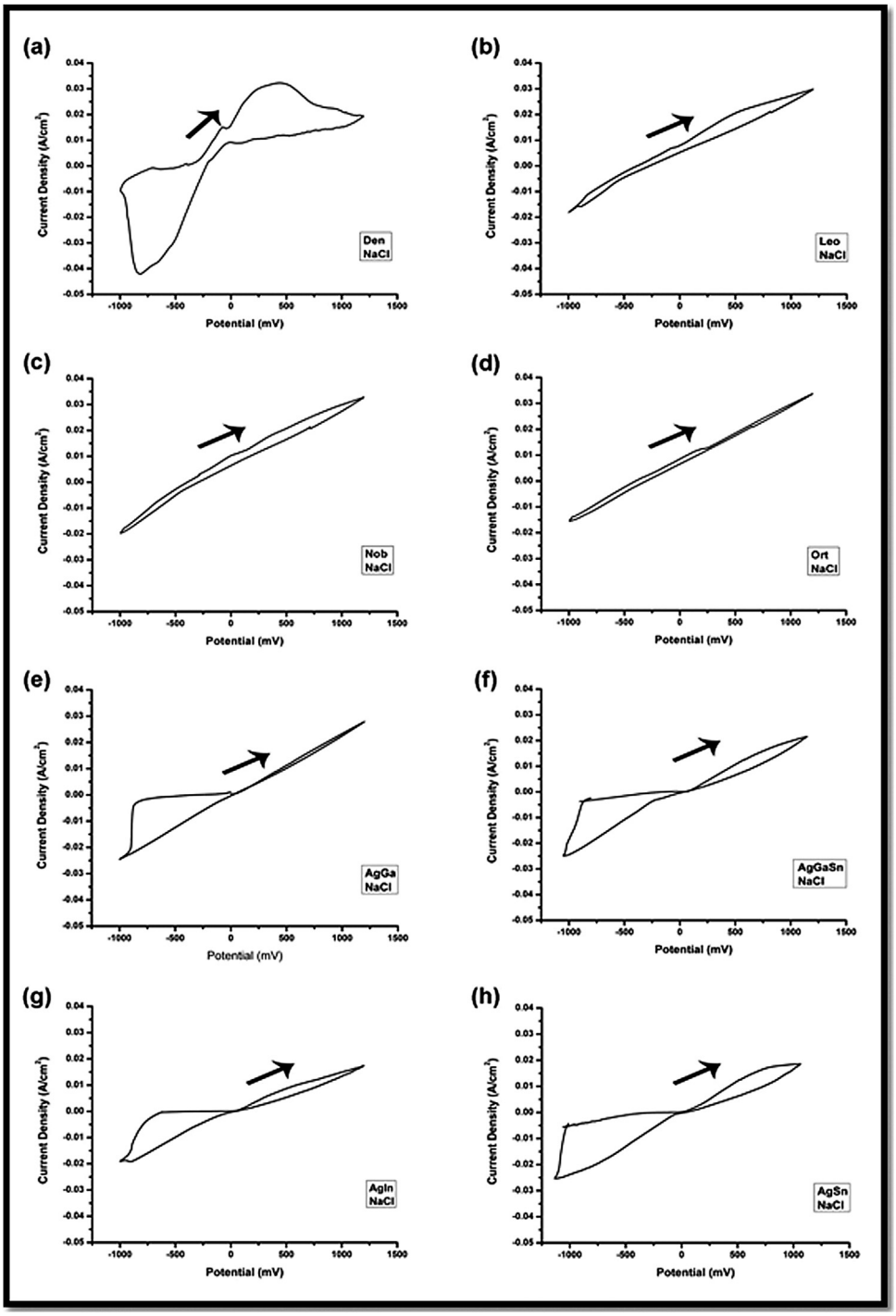

Fig. 5 – The first cycle for each alloy in NaCl solution: Den (a), Leo (b), Nob (c), Ort (d), AgGa (e), AgGaSn (f), AgIn (g), AgSn (h).

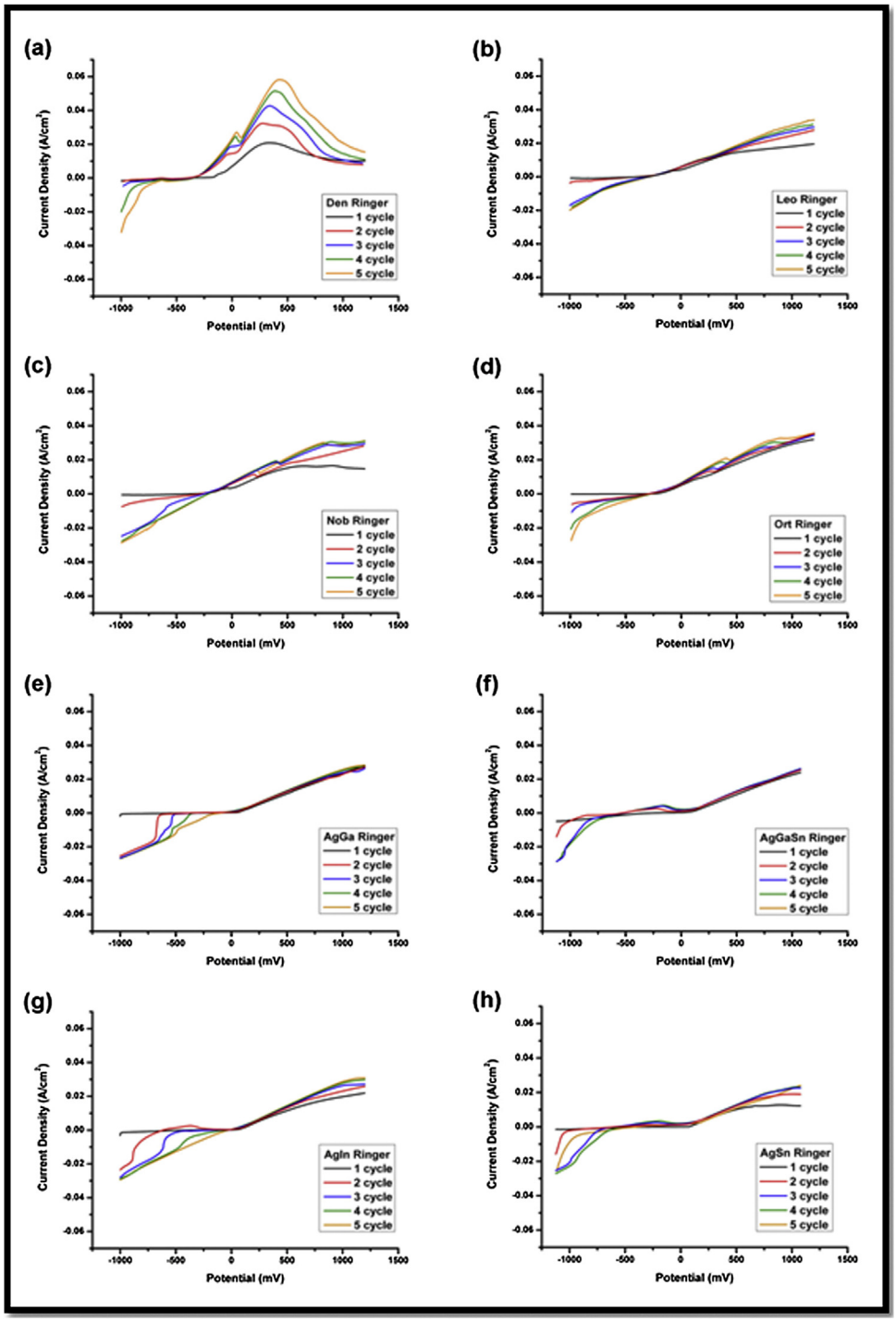

Fig. 6 – The anodic scan of the five cycles for each alloy in Ringer's solution: Den (a), Leo (b), Nob (c), Ort (d), AgGa (e), AgGaSn (f), AgIn (g), AgSn (h). The reverse scanning has been omitted for the sake of clarity.

$$Sn^{2+} + 2H_2O \Leftrightarrow Sn(OH)_2 + 2H^+ \quad (R.8)$$

$$Sn(OH)_2 \Leftrightarrow SnO + H_2O \quad (R.9)$$

$$Sn^{2+} \Leftrightarrow Sn^{4+} + 2e^- \quad (R.10)$$

$$Sn^{4+} + 4H_2O \Leftrightarrow Sn(OH)_4 + 4H^+ \quad (R.11)$$

$$Sn(OH)_4 \Leftrightarrow SnO_2 + 2H_2O \quad (R.12)$$

Apart from the oxides, Sn ions may form $SnCl_x$ due to the high concentration of Cl^- [37]. Thus the low intensity passive area corresponds to the thickening of a passive layer, which may consist of $Sn(OH)_2$, SnO, $Sn(OH)_4$, SnO_2 and $SnCl_x$ [31] which is destroyed in higher potentials.

The surface layer development on the AgGaSn (Figs. 4f and 5 f) is a combination of these for the AgGa and AgSn alloys described above. The surface layer developed can be attributed to Ga and Sn oxides and chlorides.

The passive region that develops at low potentials for the AgIn alloy (Fig. 4g and 5 h) can be attributed to an overall process described by the reaction [36,38–40]:

$$In + 3H_2O \Leftrightarrow In_2O_3 + 6H^+ + 6e^- \quad (R.13)$$

The simultaneous formation of chlorides is possible and the formation of the passive layer leads to the appearance of the passive area on the curve.

All experimental alloys demonstrate an increase slope at around 250 mV, which can be attributed to the destruction of the passive layer and the simultaneous formation of AgCl as described in (R.4).

The CP measurements show that all experimental alloys have a negative hysteresis, and thus any pits created during

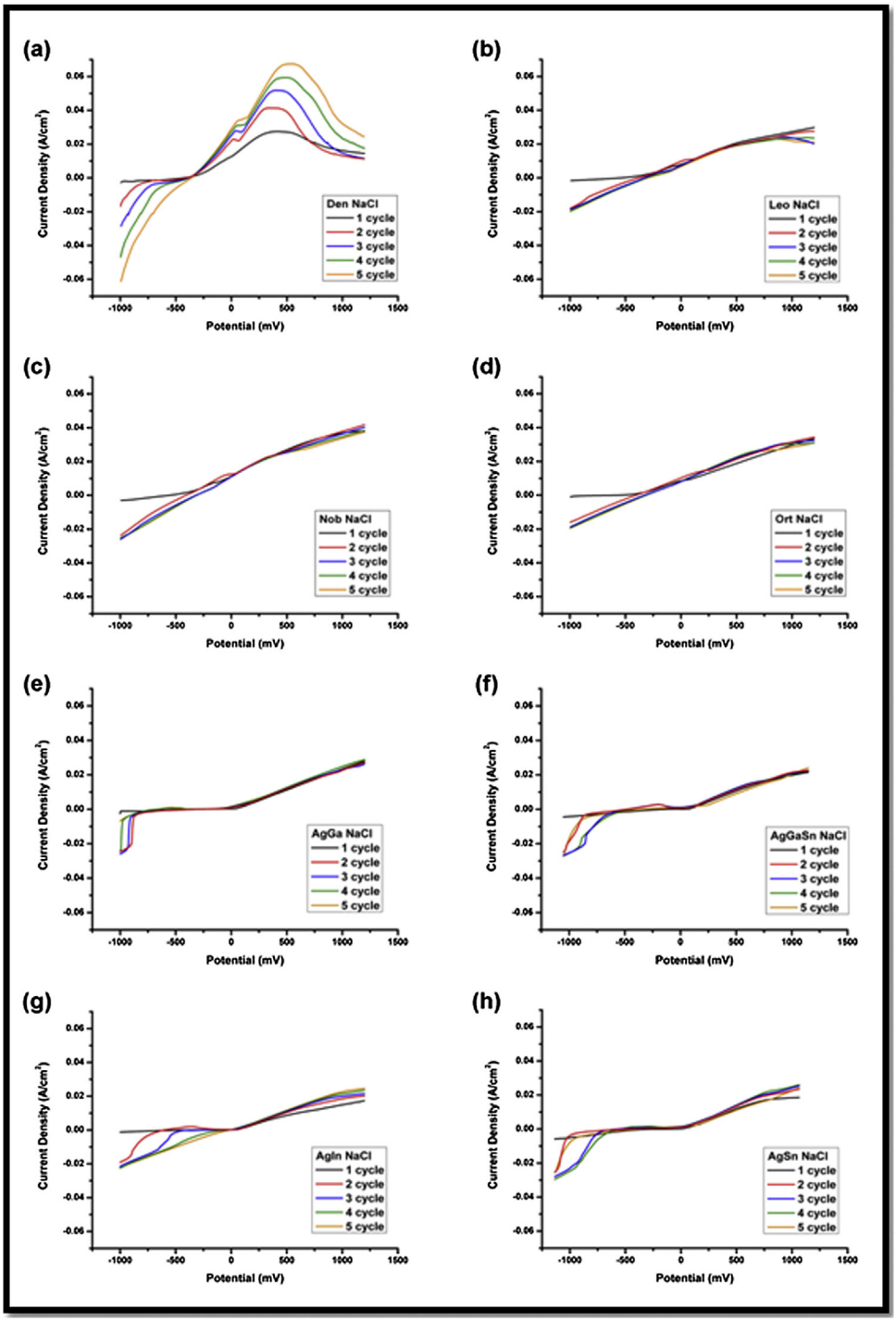

Fig. 7 – The anodic scan of the five cycles for each alloy in NaCl solution: Den (a), Leo (b), Nob (c), Ort (d), AgGa (e), AgGaSn (f), AgIn (g), AgSn (h). The reverse scanning has been omitted for the sake of clarity.

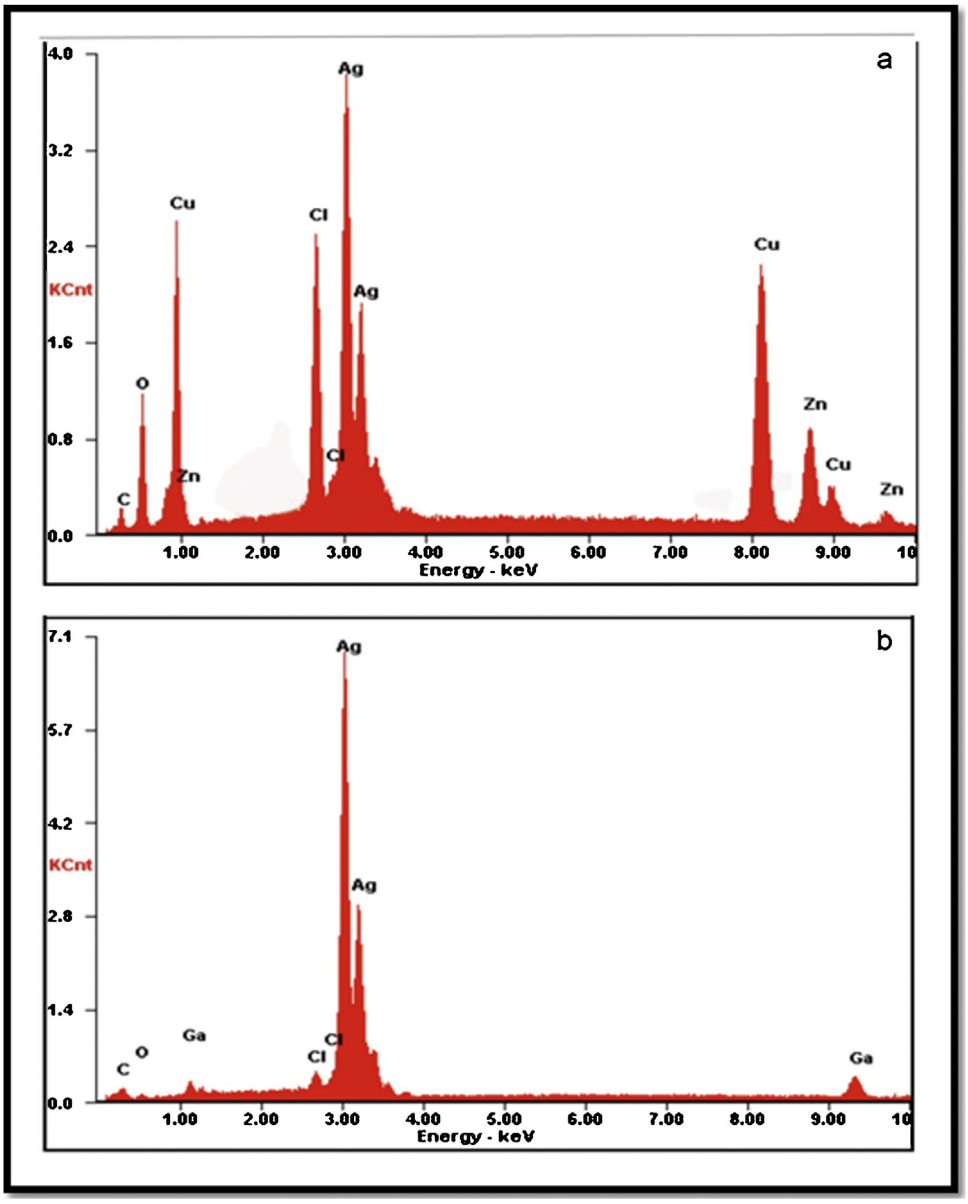

Fig. 8 – Representative EDX spectra of a commercial (a) (Den in the figure) and an experimental (b) (AgGa in the figure) alloy after CP. The presence of Cl on the surface of the specimen is evident.

anodic scanning can repair themselves. The peak identified during reverse scanning for all experimental alloys can be attributed to the reduction of the ions created in the anodic part of the voltammogram. All curves of experimental alloys demonstrate higher current magnitudes in NaCl solution, as expected for a solution stronger than Ringer's.

Only a few Nyquist plots for both solutions demonstrated a distortion from an ideal semicircle, a finding that may be attributed to surface inhomogeneity and diffusion processes. However in both solutions the commercial alloys exhibited a decreased semicircular diameter indicating a worse corrosion resistance than that for the experimental ones. Finally the greatest arc of the Nyquist plot in Ringer's solution is due to its less aggressive nature compared to NaCl.

In order to replace the existing commercially alloys with the experimental ones the ability of these alloys to join the various parts of the orthodontic devices as well as their flowability after their transformation to wires must be evaluated. Furthermore, their interaction with the oral tissues in vitro, their ionic release in vivo and their biocompatibility must be examined.

Concluding, the experimental alloys produced have better electrochemical characteristics compared to commercial ones, and this study can be the springboard for further research on the development of new Cu and Zn free Ag based brazing alloys with increased biocompatibility.

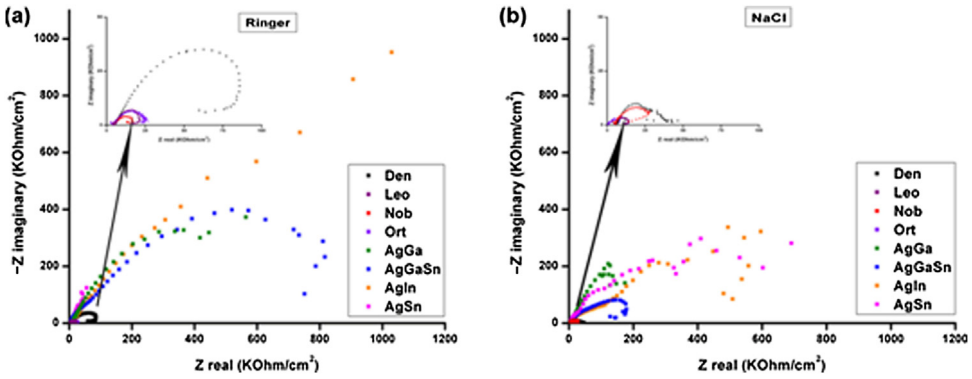

Fig. 9 – Nyquist plots for all alloys tested in Ringer's (a) and NaCl (b). Insets in a and b demonstrate a magnified view of axes origin for a better presentation of the commercially alloys tested.

5. Conclusions

- All experimental alloys demonstrated enchanced electrochemical properties compared to commercial materials.
- In and Sn have a more beneficial effect on electrochemical properties compared to Ga.

Acknowledgments

The authors extend their appreciation to the International Scientific Partnership Program (ISPP) at King Saud University for funding this research work (Grant/Award Number: ISPP# 0060).

REFERENCES

[1] Freitas MP, Oshima HM, Menezes LM. Release of toxic ions from silver solder used in orthodontics: an in-situ evaluation. Am J Orthod Dentofacial Orthop 2011;140:177–81.
[2] Zinelis S, Annousaki O, Eliades T, Makou M. Elemental composition of brazing alloys in metallic orthodontic brackets. Angle Orthod 2004;74:394–9.
[3] Soteriou D, Ntasi A, Papagiannoulis L, Eliades T, Zinelis S. Decomposition of Ag-based soldering alloys used in space maintainers after intra-oral exposure. A retrieval analysis study. Acta Odontol Scand 2012;72:130–8.
[4] House K, Sernetz F, Dymock D, Sandy JR, Ireland J. Corrosion of Orthodontic appliances-should we care? Am J Orthod Dentofacial Orthop 2008;133:584–92.
[5] Ntasi A, Al Jabbari Y, Mueller WD, Eliades G, Zinelis S. Metallurgical and electrochemical characterization of contemporary silver-based soldering alloys. Angle Orthod 2014;84:
508–15.
[6] Ntasi A, Al Jabbari YS, Silikas N, Eliades T, Zinelis S. Multitechnique characterization of conventional and experimental Ag-based brazing alloys for orthodontic applications. Dent Mater 2018;34:e25–35.
[7] Heidemann J, Witt E, Feeg M, Werz R, Pieger K. Orthodontic soldering techniques: aspects of quality assurance in the dental labaratory. J Orofac Orthop 2002;63:325–38.
[8] Berge M, Gjerdet NR, Erichsen ES. Corrosion of silver soldered orthodontic wires. Acta Odontol Scand 1982;40:75–9.
[9] Mikulewicz M, Chojnacka K. Release of metal ions from orthodontic appliances by in vitro studies: a systematic literature review. Biol Trace Elem Res 2011;139:
241–56.
[10] Mikulewicz M, Chojnacka K, Wolowiec P. Release of metal ions from fixed orthodontic appliance: an in vitro study in continuous flow system. Angle Orthod 2014;84:140–8.
[11] Staffolani N, Damiani F, Lilli C, Guerra M, Staffolani NJ, Belcastro S, et al. Ion release from orthodontic appliances. J Dent 1999;27:449–54.
[12] Vahed A, Lachman N, Knutsen RD. Failure investigation of soldered stainless steel orthodontic appliances exposed to artificial saliva. Dent Mater 2007;23:855–61.
[13] Gaetke LM, Chow CK. Copper toxicity, oxidative stress and antioxidant nutrients. Toxicology 2003;189:147–63.
[14] Haidari M, Javadi E, Kadkhodaee M, Sanati A. Enhanced susceptibility to oxidation and diminished vitamin E content of LDL from patients with stable coronary artery disease. Clin Chem 2001;47:1234–40.
[15] Bremner I. Manifestation of copper excess. Am J Clin Nutr 1998;67:1069S–73S.
[16] Kadiiska MB, Hanna PM, Jordan SJ, Mason RP. Electron spin resonance evidence for free radical generation in copper-treated vitamin E- and selenium-deficient rats:in vivo spin-trapping investigation. Mol Pharmacol 1993;44:222–7.
[17] Powell SR. The antioxidant properties of zinc. J Nutr 2000;130:1447S–54S.
[18] Kawanishi S, Inoue S, Yamamoto K. Hydroxyl radical and singlet oxygene production and DNA damage induced by carcinogenic metal compouds and hydrogen peroxide. Biol Trace Elem Res 1989;21:367–72.
[19] Press NA, editor. Panel on micronutrients, subcommittees on upper reference levels of nutrients and of interpretation and use of dietary reference intakes, intakes. atSCotSEoDR. Dietary reference intakes for vitamin A, vitamin K, arsenic, boron, chromium, copper, iodine, iron, maganese, molybdenium, nickel, silicon, vanadium and zinc. Washington D.C: National Academy of Sciences; 2000.
[20] Borovansky J, Riley PA. Cytotoxicity of zinc in vitro. Chem Biol Interact 1989;69:279–91.
[21] Meryon SD, Jakeman KJ. The effects in vitro of zinc released from dental restorative materials. Int Endod J 1985;18:191–8.
[22] Tulonuglu O, Ulusu T, Genc Y. An evaluation of survival of space maintainers: A six year follow up study. J Contemp Dent Pr 2005;6:1–8.
[23] Rajab LD. Clinical performance and survival of space maintainers: evaluation over a period of 5 years. J Dent Child 2002;69:156–60.
[24] Baroni C, Franchini A, Rimondini L. Survival of different types of space maintainers. Pediatr Dent 1994;16:360–1.

[25] Qudeimat MA, Fayle SS. The longevity of space maintainers: a restrospective study. Pediat Dent 1998;20:267–72.
[26] Tunk ES, Bayrak S, Tuloglu N, Egilmez T, Isci D. Evaluation of survival of 3 different fixed space maintainers. Pediatr Dent 2012;34:97–102.
[27] Fathian M, Kennedy DB, Nouri MR. Labaratory-made space maintainers: A 7-year retrospetive study from private pediatric dental practice. Pediatr Dent 2006;29:500–6.
[28] Beverskog B, Puigdomenech I. Revised pourbaix diagrams for copper at 25 to 300 degrees C. J Electrochem Soc 1997;144:3476–83.
[29] Gao YF, Cheng CQ, Zhao J, Wang LH, Li XG. Electrochemical corrosion of Sn-0.75Cu solder joints in NaCl solution. Trans Nonferrous Met Soc China 2012;22:977–82.
[30] Al-Mobarak NA. Cyclic voltammetry study of passivation of tin in sodium dihydrogen phosphate solution. Chem Tech Fuels Oil 2012;48:321–30.
[31] Metikos-Hukovic M, Omanovic S, Jukic A. Impedance spectroscopy of semiconducting films on tin electrodes. Electrochim Acta 1999;45:977–86.
[32] Rehim SSA, Sayyah SM, El Deeb MM. Corrosion of tin in citric acid solution and the effect of some inorganic anios. Mater Chem Phys 2003;80:696–703.
[33] Hassan HH, Ibrahim MAM, Abd El Rehim SS, Amin MA. Comparative studies of the electrochemical behavior of silver electrode in chloride, bromide and iodide aqueous solutions. Int J Electrochem Sci 2010;5:278–94.
[34] Mueller WD, Schoepf C, Nascimento ML, Carvalho AC, Moisel M, Schenk A, et al. Electrochemical characterization of dental alloy: its possibilities and limitations. Anal Bioanal Chem 2005;381:1520–5.
[35] Horasawa N, Nakajima H, Takahashi S, Okabe T. Behavior of pure Gallium in water and various saline solutions. Dent Mater 1997;16:200–8.
[36] Metikos-Hukovic M, Omanovic S. Thin indium oxide film formation and growth: impedance spectroscopy and cyclic voltammetry investigations. J Electroanal Chem (Lausanne) 1998;455:181–9.
[37] Keller P, Strehblow H-H. Passivity of Tin and CuSn alloys in alkaline media studied by X-ray photoelectron spectroscopy. In: Marcus P, Maurice V, editors. Passivation of metals and semiconductors, and properties of thin oxide layers. Paris, France: Elsevier; 2006. p. 137–42.
[38] El-Sayed A-R, Mohran HS, El-Lateef HMA. Potentiodynamic studies on anodic dissolution and passivation of tin, indium and tin-indium alloys in some fruit acids solutions. Corros Sci 2009;51:2675–84.
[39] Hattori M, Tokizaki T, Matsumoto M, Oda Y. Corrosion properties of Ag-Au-Cu-Pd system alloys containing indium. Bull Tokyo Dent Coll 2010;51:7–13.
[40] Omanovic S, Metikos-Hukovic M. Thin oxide films on indium: impedance spectroscopy investigation of reductive decomposition. Thin Solid Films 1995;266:31–7.